International Journal of
INTELLIGENT SYSTEMS AND APPLICATIONS IN ENGINEERING
ISSN:2147-6799 www.ijisae.org Original Research Paper

An Efficient Image Segmentation using Optimized Segmentation Network for Remote Sensing Satellite Images

Namdeo Baban Badhe[1], Vinayak Ashok Bharadi[2], Nupur Giri[3], Sujata Alegavi[4], Shashank S. Tolye[5]

Submitted: 22/04/2023 **Revised**: 27/06/2023 **Accepted**: 15/07/2023

Abstract: Segmentation of high-resolution remote sensing images is of great importance for urban development planning. Moreover, while monitoring land covers through high-resolution satellite images, crops are significantly easy to be confused with the dark object's spectra like, shadows, dense vegetation and asphalt roads. The previous semantic segmentation approaches do not pay enough attention to the location information among horizontal position and direction, which causes inaccurate segmentation of remote sensing images. To overcome these issues, an innovative Optimized Segmentation Network (OptSegNet) based remote sensing image segmentation is proposed which is a hybridization of convolutional network and dual-path UNet with Resnet_50. It consists of four stages such as, pre-processing, feature extraction, segmentation and post processing. Initially, the hyperspectral images which are derived from the Indian Pines dataset, Salinas, and Pavia University are preprocessed by using the guided box filtering technique. Secondly, the proposed method extracts the spatial and spectral features from the satellite images and also generates accurate segmentation results. In order to enhance the performance of proposed method, Enhanced Mountain Gazelle Optimization (EMGO) algorithm is used. Finally, in the post processing stage the proposed pairwise neural conditional random field method enhances the final segmented images into a high-resolution remote sensing image. Experimental outcomes illustrate that the introduced method achieves better performance when compared with the other traditional algorithms. Especially, the accomplished overall accuracy is 99.13%, 99.71%, and 99.34% on Indian Pines dataset, Salinas, and Pavia University dataset respectively.

Keywords: *Image segmentation, spectral and spatial features, semantic segmentation, remote sensing, convolutional neural network*

1. Introduction

Recently, it has been possible to gather a number of remote sensing images. For example, Indian Pines (IP), Salinas Dataset (SD) (Salinas Scene), and Pavia University (PU) consists of huge number of satellite images along with maximum spatial resolution. These images have provided several more capability for image analysis works like semantic segmentation, scene classification, and change detection. Among these works, Remote Sensing Image's (RSI) semantic segmentation is one of the most significant and interesting research domains because it is broadly applied in several applications, like city planning, environmental monitoring dense labeling, urban management. Urban planning, RS mapping precision agriculture, landscape classification, environmental protection against climate change, and forest vegetation are just a few areas where Remote Sensing (RS) image segmentation technology is essential [1-3].

As a result, it offers crucial decision assistance for everyday activities of people. The goal of semantic segmentation of RSI is to categorize each pixel's land-cover or land-use. Semantic segmentation has gained considerable interest in the remote sensing industry as one of the core visual tasks and has shown to be helpful for a number of applications, including mapping the land cover, observing traffic, and managing urban areas [4-7]. Convolutional Neural Network (CNN) plays a significant role in the semantic segmentation of RSIs. Various CNN systems like DeepLab and its variants performs the sematic image segmentation efficiently. Although, these systems face some challenges because this CNN-based structure are more sensitive to the features of both training and testing images. Also, the segmentation accuracy gets minimized severely because of the various distributions of input and output images.

Semi supervised learning algorithms are suggested to employ additional information, such as spatial relations for semantic segmentation, in order to reduce the need for detailed pixel-by-pixel annotations. However, majority of work does not discuss about the interpret of spatial relationships between RS objects, that restricts the comprehension of these objects,

[1]*Research Scholar, Department of Information Technology, Finolex Academy of Management and Technology, P-60, P-60/1, MIDC, Mirjole Block, Ratnagiri, Maharashtra 415639, India*
Email: namdeobadhe1982@gmail.com
[2]*HOD & Professor, Department of Information Technology, Finolex Academy of Management and Technology, MIDC, Mirjole Block, Ratnagiri, Maharashtra 415639, India*
Email: vinayak.bharadi@famt.ac.in
[3]*HOD & Professor, Department of Computer Engineering, Vivekanand Education Society's Institute of Technology, Hashu Adwani Memorial Complex, Collector's Colony, Chembur, Mumbai, Maharashtra 400074, India*
Email: nupur.giri@ves.ac.in
[4]*Associate Professor, Head of the BTech Internet of Things Department, Thakur College Engineering and Technology, Kandivali - (East), Mumbai – 40010, India*
Email: sujata.dubal@thakureducation.org
[5]*Professor, Finolex Academy of Management and Technology, MIDC, Mirjole Block, Ratnagiri, Maharashtra – 415639, India*
Email: shashank.tolye@famt.ac.in

particularly when the phenomena of several remote sensing objects have the same spectrum emerges. In RS, the occurrence of various objects with the same spectrum is rather typical [8-10]. Only using an object's own textures, spectra, and shape information is challenging. To aid in making decisions, object detection involves multi-scale semantic data and geographically neighboring items. When distinct things have the same spectrum, the spatial relationship between remote sensing objects is crucial to their identification [11-13].

The RS image provides a significant quantity of information due to the RSI improved resolution, which broadens their application potential and causes recognized items of interest to be relatively smaller in size [14, 15]. The methods for segmenting images are the main topic of this section. Partitioning remote sensing imagery into discrete earth surface regions and creating a labelled map are typical image analysis goals. The major contributions of this proposed work are given as follow:

- An OptSegNet based segmentation is introduced, based on this method, a dual UNet with ResNet_50 sub network is designed to fully interpret the semantic information of RSIs.
- Depth-wise convolution is designed in the proposed segmentation module to extract the joint SSF further; it enhances the effectiveness of the extracted global features.
- It also enhances, semantic segmentation of RSIs by improving the scene-based representation in both ResNet_50 encoder and ResNet_50 decoder stages.

The rest of this research work is provided as follows. Part 2 discusses about some of the state-of-art techniques that are related to this work. Part 3 discusses the proposed system. Part 4 provides the results and part 5 is the conclusion of this work.

2. Literature Survey

The sate-of-art techniques based on RSI segmentation and classification are discussed in this section.

In 2023, Zhou et al., [16] had proposed a Shallow-to-Deep Feature Enhancement (SDFE) system with various modules depends on Vision Transformer (ViT) and CNN is introduced. Initially, Principal Component Analysis (PCA) was developed for selecting the significant spectral context. Next, the spatial and spectral correlations are preserved by using 3D-CNN based Shallow SSF extraction (SSSF). Then, the complementary information was captured by 2D-CNN. At last, ViT module extracts the joint SSFs for segmentation. The disadvantage of this model was, network structure enhancement is required to achieve more efficient outcomes.

In 2022, Zhao et al., [17] had introduced a graph learning scheme for the classification of Hyperspectral Image (HSI). The choosing of improper segmentation scale greatly minimized by multiscale-superpixel based system. The final segmentation-based classification results was achieved with the help of pixel-level fusion approach. But the only drawback of this system was, the computational complexity is high, if the HSI is in larger size.

In 2022, Kondal and Barpanda [18] had developed Hybrid 3D-CNN (H3D-CNN) system for accurate HSI classification in supervised learning. The 2D-CNN's HSI consists of hundreds of spectral dimensions which maximizes the computational expenses. So, there is a need for dimensional suppression. To overcome this issue, the proposed H3D-CNN system with two convolution layers provides better results. But the only disadvantage was, the unmarked samples may reduce the robustness of the introduced framework.

In 2022, Song et al., [19] had implements Semi-Supervised Residual Network (SSRNet) system for classification. It includes two classes, SS and a self-supervised branch. By using HSI data perturbation through a spectral spatial shift, the SS branch enhances the performance. Further, the self-supervised branch describes band reconstruction. SSRNet perform better on unlabeled samples which enhances the classification accuracy. The only disadvantage was several unlabeled samples are applied to enhance the performance it increases the training time of the process.

In 2022, Zhang et al., [20] had introduced Superpixel NonLocal Weighting Joint Sparse Representation Classification (SNLW-JSRC). The entropy rate segmentation approach was used for constructing superpixel representation of an image. To weigh the superpixel, proposed SNLW strategy is constructed which is done based on its spectral and structural informations. At last, the superpixel based classification is performed with the aid of JSRC approach. The drawback of this system was, the inaccurate superpixel segmentation causes lack of spatial information.

In 2019, Chakraborty et al., [21] had introduced an Improved Particle Swarm Optimization (IPSO) to solve the issue of premature convergence and also escapes from the local optima problem. It is extended further to replace the worst particles with the help of fitness particles. In the experimental scenario, it is compared with some of the optimization methods like, FireFly (FF), Differential Evolution (DE), and Cuckoo Search (CS). The drawback was, some of the parameters need to be modified to increase the accuracy of segmentation results.

In 2020, Wang et al., [22] had proposed sequential joint DL model for the HSI segmentation and classification. Initially, hybrid the attention scheme to distribute the key feature's probability weight. Then, a multiscale convolution method was used to obtain deep features. The Bidirectional Long Short-Term Memory (Bi-LSTM) classifies the multiclass RSIs accurately. The major disadvantage was, convergence

visualization analysis was performed to understand the training outcomes better.

In 2021, He et al., [23] had introduced spectral-spatial segmentation-based classification by applying label dependence. Initially, residual network is applied to extract the spectral features, next the target pixels are fed into pixel embedding by using label dependency characteristics. Finally, the Spatial Information Extractor (SIE) extracts the spatial dependency information efficiently which provides better segmentation-based classification outcomes. The only drawback was, it requires larger training time which leads to imperfect features learned by the system.

In 2022, Datta et al., [39] had introduced a hybrid Spatial-Spectral-Superpixelwise Principle Component Analysis-based Dense 2D-3D CNN (3SPCA-D-2D-3D-CNN) technique for dimensionality reduction and classification of HSI. It is build-up of nine enriched features with the aid of these features, the appropriate class labels are classified. The only disadvantage was, the hyperparameters are not optimized by using any optimization algorithm.

In 2022, Mu et al., [40] had introduced a Two-Branch CNN based on Multi-spectral Entropy Rate Superpixel (TBN-MERS) for HSI segmentation and classification. It uses the joint Spatial-Spectral Features (SSF) for the efficient classification performance. The drawback of this method was, to design deep neural network to enhance the segmentation results.

Research motivation

From the above-mentioned existing methods, generating labeled training data consumes lot of time and also limited amount of training samples are available which makes the segmentation
more complex. Further, the existing CNN is used directly, however this has certain drawbacks, including poor segmentation of tiny objects and fuzzy boundaries. The shallow and deep feature map is partially combined using this method; however, the fusion is not selective. The capacity to extract features is limited even if the shallow network structure has more detailed information because of the small number of network layers and the convolutions that was made. The effect of segmentation is limited by the improper patch size, feature map's significant noise and high processing time. These are motivated to do this research work based on RSI segmentation technique.

3. Proposed Methodology

One of the most difficult and crucial problems in the fields of vision and RS has been semantic segmentation of RSIs. It is widely used in several disciplines, including urban development, environmental monitoring, and land surveying and mapping. RSI typically include a wealth of information about many categories of ground objects. Due to the heterogeneity of linked objects and the complicated spectrum in satellite images, segmenting remote sensing images involves a high deal of uncertainty, which severely restricts the effectiveness of typical segmentation techniques. In this research work, OptSegNet based RSI segmentation is proposed. Fig. 1 represents the process flow of proposed system.

The proposed method contains 4 stages, (1) preprocessing, (2) feature extraction (3) segmentation and (4) post preprocessing.

Initially the input RSIs are taken from, HSI dataset such as IP, SD, and PU. Secondly, these images are preprocessed by guided box filtering. Then, given to the OptSegNet for feature extraction and segmentation.

To enhance the OptSegNet's performance, EMGO is utilized. Then the segmented image is given to Pairwise Neural Conditional Random Field (PNCRF) based post processing for improving the segmentation accuracy.

Finally, the introduced model is compared with various previous models to illustrates the effectiveness of the introduced feature extraction-based segmentation algorithm.

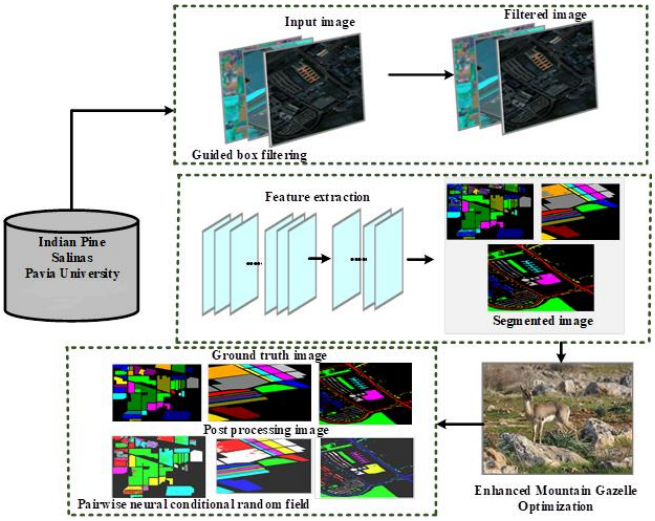

Fig 1. Proposed Methodology

3.1. Guided Box Filtering (GBF) for preprocessing the HSIs

It is a local linear filtering method, which smoothens the RSI by considering the average-of-surrounding pixels. This GBF technique applies summed area table and square kernel strategy which calculate the box filtering kernel independently [24]. The summation method is used to calculate the cumulative sum over x-axis and y-axis. It is mathematically written in equations (1) and (2)

$$S(x,y)=S(x-1,y)+L(x+v)-L(x-v-1,y) \quad (1)$$

$$K(x,y)=K(x,y-1)+S(x,y+v)-S(x,y-v-1) \quad (2)$$

where, S,L and K are the variables, v specifies the vector. Finally, the result of box filter is mentioned in equation (3),

$$Box(x,y)=\frac{1}{(2v+1)^2}k(x,y) \tag{3}$$

where, k denotes the cardinality of K. While recovering the edge in both discrete and gradient region, the Guided Image Filter (GIF) method is highly suitable. The resultant of the color guidance filtering is given in equations (4-7)

$$GBF=\tilde{p}_b^T I_i+\tilde{q}_b \tag{4}$$

$$\tilde{p}_b=\frac{1}{|w|}\sum_{r\in w_i}p_r \quad \tilde{q}_b=\frac{1}{|w|}\sum_{r\in w_i}q_r \tag{5}$$

$$p_r=(\Sigma_r+eH)^{-1}\left(\frac{1}{|w|}\sum_{i\in\omega_r}I_iL_i-m_r\tilde{I}_r\right) \tag{6}$$

$$q_r=\tilde{I}_r-p_r^T m_r \tag{7}$$

where, l be the input image, b denotes the set of pixels, T specifies the linear coefficient, H represents the variables, the average of input RSI is represented as $\tilde{I}_r$, the average of guidance RSI is denoted as m_r, e be the controlling parameter, the guided image's 3×3 covariance matrix in w_r is represented as Σ_r, the linear coefficient is represented as $\tilde{q}_r$ and $\tilde{p}_r$, the parameter H is denoted as 3×3 identity matrix, r be the radius of 5 and e be the epsilon value as 0.1. Integration of guided filtering and box provides excellent outcomes and also it preserves the structure information in a RSI.

3.2. OptSegNet based feature extraction and segmentation

The proposed OptSegNet is the hybridization of convolutional network based dual-path U-net with Resnet. It is used for feature extraction and segmentation of RSIs. This proposed architecture includes two UNet i.e. UNet1 and UNet2 and an encoder block ResNet_50 sub network. The dual UNet with ResNet encoder differentiate it from UNet by means of ResNet_50, Decoder Block (DB) and ASPP applications in UNet1. Among the outcomes of UNet1, an element by element multiplication is performed along with the same network's input. In UNet2, the employ of ASPP, is the major difference between dual UNet with ResNet encoder and UNet. If the encoder in UNet2 was generated from the starting, in dual UNet with ResNet encoder, the very first encoder purposes pre-trained ResNet_50. The two 3×3 convolution functions are performed in the UNet2 encoder, each of which is followed by a batch normalization. Rectified Linear Unit (ReLU) is used as the activation function, it is achieved with the aid of excitation block and squeeze, enhancing the integrity of the feature maps significantly. To reduce the feature map's spatial dimension, max-pooling is used after the application of 2×2 window and stride2. Set the depth-wise convolutional kernel size as 13×13 to achieve appropriate result. In dual UNet with ResNet encoder, there are two decoders are applied. For each block, the input feature map is subjected to a 2×2 bi-linear up sampling in the decoder region. It greatly maximizes the input feature map's dimensionality. From the encoder, the respective skip connections integrate the feature maps with the resultant feature maps. In the first decoder, only, the encoder's skip connections in UNet1 is applied, while the skip connection from UNet1 and UNet2 encoders are applied in second DB. After concatenation, two 3×3 convolution functions are done, each attained by a ReLU function and batch normalization. Then, an excitation and squeeze block are used. Finally, a convolution layer with sigmoid function is used which produces the segmented result as the output [25]. Then, the EMGO algorithm minimizes the loss of dual UNet with ResNet_50 network which is mentioned in equation (8).

$$L_E=\left|\left(x_j\times\log p_j\right)+\left(1-x_j\right)\times\log\left(1-p_j\right)\right| \tag{8}$$

where, L_E denotes the cross-entropy loss, x_j represents the ground truth label 1, the term $1-x_j$ denotes ground truth label 0 and the classifier probability is mentioned as p_j. Fig. 2 illustrates the architecture of dual UNet with ResNet_50 model.

3.2.1. Enhanced Mountain Gazelle Optimization (EMGO) for improving OptSegNet performance

In this section, an optimization approach based on life and social behaviors of mountain gazelles is performed. To form a mathematical equation for the MGO approach, the general concepts of group and social life of mountain gazelles are applied. The MGO algorithm performs optimization functions depends on four major factors, such as Territorial Solitary Males (TSM), Maternity Herds (MH), Bachelor Male Herds (BMH), and Migration to Search for Food (MSF).

In the search space, the positions of mountain gazelle are distributed randomly. If there are no neighboring particles around the present particle, it performs random walk scheme. This state slow down the convergence trend and minimizes the accuracy of convergence under some finite amount of iterations. An enhanced learning factor is proposed to overcome this problem and the relative change rate of the mountain gazelle's fitness value is proposed which is mention in equation (9).

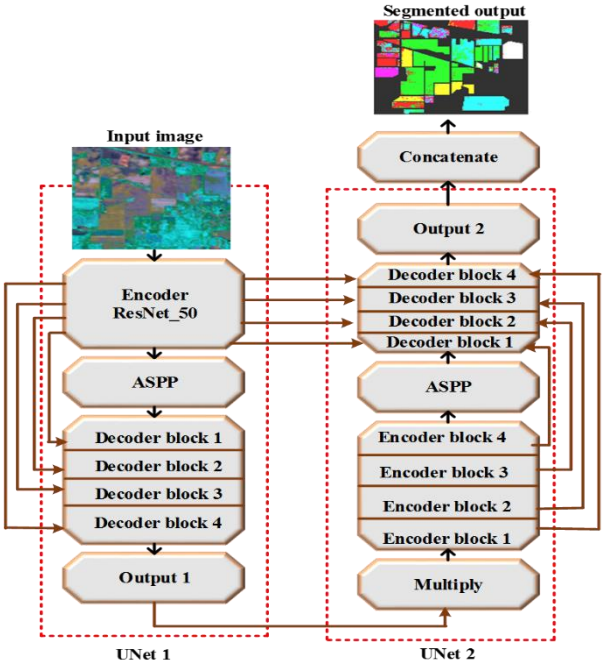

Fig 2. Architecture of proposed OSegNet

Pseudo Code for EMGO:

ıputs: Population size M and the T be the maximum number f iterations

utputs: Fitness value and location of mountain gazelle

ıitialization

pplying $P_i(i=1,2,\ldots,M)$ to form a random population

ompute fitness levels of mountain gazelle

$$Fitness\_Function = Minimization(L_E) \quad (10)$$

/hile (termination constraint is not reached) do

ır (every gazelle (P_i)) do

lone male realm

valuate TSM by applying,

$$T_{SM} = male_{gaz} - |(si_1 \times YM - si_2 \times P(t)) \times D| \times Coe_S \quad (11)$$

lother and child herd

valuate MH by applying,

$$M_H = (YM + coe_{1,s}) + (si_3 \times male_{gaz} - si_4 \times P_{rand}) \times coe_{1,s} \quad (12)$$

oung male herd

valuate BMH by applying,

$$B_{MH} = (P(t) - F) + (si_5 \times male_{gaz} - si_6 \times YM) \times coe_s \quad (13)$$

ligration to search for food

valuate MSF by applying,

$$M_{SF} = (UB - LB) \times s_7 - LB \quad (14)$$

ompute the fitness values of MH, TSM, MSF, and BMH, ıen add them to the habitat

rrange the total population in ascending order

daptive learning factor

$$a_i^t = \frac{1}{1+e^{-\upsilon}} \quad (15)$$

eighbor individual gazelle around

$$b = -1 + Iteration \times a_i^t\left(\frac{-1}{MaximumIteration}\right) \quad i = 1,2,\ldots,t$$
$$b = -1 + Iteration \times coe_i\left(a_i^t\left(\frac{-1}{MaximumIteration}\right)\right) \quad else \quad (16)$$

pdate $best_{gaze}$

tore the M best gazelles $Maximum$ number of populations

eturn $P_{best\ gaze}$, optimal fitness.

$$e = \frac{\left|F\left(male_i^t\right) - F\left(male_{best}^t\right)\right|}{F\left(male_{best}^t\right) + \lambda} \quad (9)$$

where, $male_{gazelle}^t$ denotes the i^{th} individual of the mountain gazelle at the iteration t, $F\left(male_i^t\right)$ is the fitness function, $F\left(male_{best}^t\right)$ represents the achieved optimal fitness rate of mountain gazelle and λ signifies the constant value to eliminate zero-division-error. Table 1 illustrates the pseudo code for EMGO [26].

where, P signifies the random population, si be the random integers ranges from (1-6), YM denotes the young male herd, D represents the coefficient, coe_S signifies the randomly chosen coefficient vector, P_{rand} is the gazelle's vector position, $P(t)$ is the gazelle position, $UB - LB$ denotes the upper and lower limits, and a denotes the adaptive factor.

3.3. Pairwise neural conditional random field-based post processing

During the data transfer between the neural network layers, some context information may get lost, along with attaining high-level spatial features. Thus, the segmentation outcomes produced by the OSegNet approach may result in several flaws, particularly at the boundaries of ground objects. To resolve these defects, the CRF strategy is used in the computer vision research domain. It is performed usually in the post-processing step to enhance the resultant segmented

RSIs [27]. The mathematical model for CRF is given in equation (17),

$$Q(P|R)=\frac{1}{N(R)}\exp\left(-\sum_{a\in A_g}\log(P_A|R)\right) \quad (17)$$

where P denotes a set of random variables $\{p_1, p_2,\ldots, p_M\}$ where p_M be the M^{th} pixel's category label, R signifies a group of random variables $\{R_1, R_2,\ldots, R_M\}$, the pixel vector is represented as R_M, the normalizing factor is represented as $N(R)$, the clique is given as a, set of cliques is represented as A_g, and g induces a potential ϕ_a. By computing CRF expression, it adjusts every pixel's category label and attains the objective of correcting the resultant segmented RSIs. This CRF post processing method is significantly efficient at processing RSIs which consists of small number of objects only. Therefore, the locations, sizes, and number of objects vary widely in RSIs and the conventional CRF performs a global optimization of the whole image. In the similar way, various portions of ground objects which are not shadowed or shadowed are processed which causes more errors in the outcome of CRF. Therefore, a PNCRF method is proposed which overcomes the disadvantages of inconsistent and noisy labeling from the CRF alone.

In PNCRF, the pairwised image I is mathematically mentioned in equation (18),

$$I=\eta(a_i,b_j)\underbrace{\sum_{n=1}^{N} w^{(n)}r^{(n)}(v_i,v_j)}_{r(v_i,v_j)} \quad (18)$$

where, the learnable parameters are $w^{(n)}$, the number of kernels are denoted as N, the parameter v_i be the feature vector of i^{th} pixel and v_j be the feature vector of j^{th} pixel, the operation $\eta(a_i,b_j)$ denotes the compatibility transformation among the labels a_i and a_j. The achieved post processing result is mentioned in equation (19).

$$PostProcessOutcome=I_{seg'}^{\gamma} \quad (19)$$

where $I_{seg'}^{\gamma}$ represents the segmented output, and γ represents the range $[1,\gamma]$. This proposed PNCRF method only uses shallow features which produces more effective post processing RSI results.

Initially, the hyperspectral RSIs are pre-processed by using a GBF technique. Secondly, the OptSegNet extracts the spatial and spectral features then provides the segmentation outcomes. Finally, the PNCRF further enhances the segmented images respectively.

4. Results and Analysis

The experimental setup of the introduced approach and the obtained results comparison are discussed briefly in this section.

Experimental setup

The experiments were run on Spyder Anaconda Navigator with python 3.10 version with 16.0 GB and on Intel(R) Core (TM) i7-6700 CPU @ 3.40GHz 3.40 GHz processor, Windows 10 operating system. After the completion of network design, analyzed the various factors which affects the system performance and training process. These factors consist of number of epochs, number of iterations and learning rate. Set the learning rate at 0.001, and number of iterations at 100. The network weighs were initialized and trained randomly by EMGO algorithm with an entropy loss function. Every experiment was run for 200 epochs. For an efficient comparison with other existing methods, adopt a patch size of 13×13. The proposed OSegNet model was constructed using the Keras and Torch library.

Performance analysis

The description of three experimental databases such as IP, SD, and PU dataset are introduced. After that, the outcomes of the introduced approach and some other related techniques on different datasets are discussed. The existing methods which are compared with the proposed work are: 3D-CNN, and 2D-CNN [18], HybridSN [16], Spectral-CNN, IPSO, CS, DE, FF [21], AlexNet, ResNet, DenseNet, Pre-activation Residual Attention Network (PRAN), and FSSFNet [22, 23] respectively.

(i)

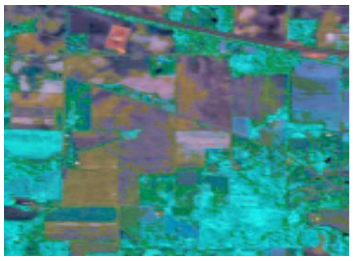

(ii)

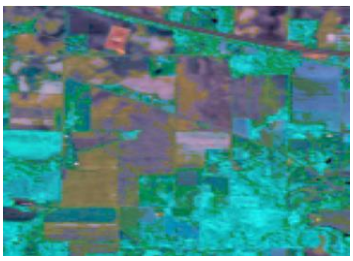

(iii)

(iv) (v)

Fig 3. Results of the proposed approach on Indian Pines Dataset

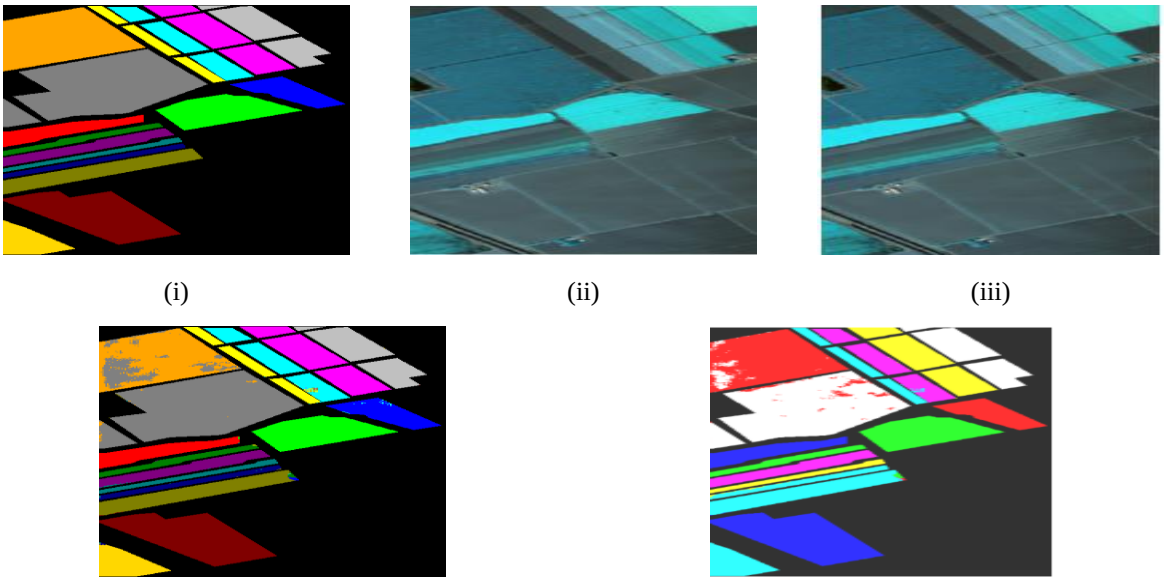

(i) (ii) (iii)

(iv) (v)

Fig 4. Results of the introduced method on Salinas Scene Dataset

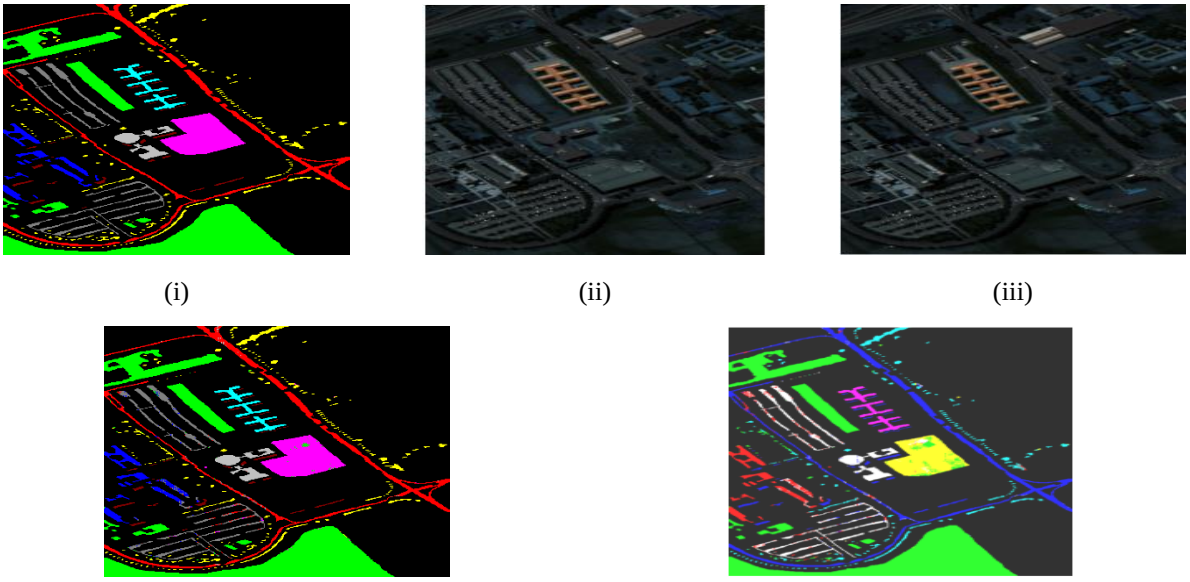

(i) (ii) (iii)

(iv) (v)

Fig 5. Results of the proposed approach on Pavia University Dataset

Fig. 3 illustrates the segmentation result of the proposed method on IP; (i) Ground truth image, (ii) RGB converted image (iii) Filtered image (iv) Segmented image and (v) Post-processing image.

Fig.4 demonstrates the segmentation result of the introduced model on SD; (i) Ground truth image, (ii) RGB converted image (iii) Filtered image (iv) Segmented image and (v) Post-processing image.

Fig.5 illustrates the segmentation result of the introduced method on PU; (i) Ground truth image, (ii) RGB converted image (iii) Filtered image (iv) Segmented image and (v) Post-processing image.

4.1. Dataset description

Three HSI databases are chosen for analysis, such as IP, SD and PU. The detailed description of these three datasets are as follows,

Indian Pine dataset

The IP database contains spectral channels of 200, $145*145$ pixels in the wavelength of range 0.4-2.45 μm. The data's spatial resolution is 20 m. The ground truth map uses 16 various surfaces classes and 10,249 labeled pixels [28].

Salina dataset

The SD consists of 512×217 pixels along with a 3.7 m spatial resolution and 200 spectral channels (0.4-2.45 μm). It also consists of 16 classes and the ground truth of 54,129 labeled pixels [29].

Pavia University

The PU dataset's spatial size and resolution is 610×340 and $1.3m/pixel$ respectively. It also consists of 115 spectral channels ($0.43-0.86\mu m$). The ground truth image includes 42,776 labeled pixels and 9 classes [30].

4.1.1. Comparison of classification models

Table 2 represents the various existing methods applied in IP and SD at the various convolution layers.

Table 2. Classification Accuracy Based on India Pines Dataset, Salinas Dataset and Pavia University Dataset

Class Labels	Methods				
	3D-CNN [18]	2D-CNN [18]	ybrid SN [16]	pectral CNN	Proposed
Indian Pines Dataset					
Alfalfa	35.71	71.72	00.00	00.00	100
Corn-notill	96.46	95.85	7.82	3.3	98.68
Corn-mintill	97.13	95.90	5.45	5.39	98.78
Corn	98.55	73.91	5.71	7.23	99.39
Grass-pasture	97.90	97.20	9.54	9.50	98.20
Grass-trees	97.68	96.31	9.85	9.85	99.80
Grass-pasture-mowed	100	100	0	9.98	39.47
Hay-windrowed	99.30	100	00.00	9.96	100
Oats	100	100	00	00	71.42
Soybean-notill	98.26	97.20	5.46	7.95	99.70
Soybean-mintill	98.77	99.04	7.33	3.56	99.76
Soybean-clean	97.15	95.45	5.07	7.89	97.07
Wheat	96.72	100	7.30	9.04	100
Woods	99.46	98.94	9.21	00	100
Buildings-Grass-Trees-Drives	93.80	94.73	00	9.95	97.75
Stone-Steel-Towers	100	100	9.76	7.45	95.31
Overall Accuracy (OA)%	97.31	96.37	7.57	3.06	99.13
Average Accuracy (AA)%	98.92	97.08	4.72	5.17	99.58

Kappa%	-	-	7.23	7.29	99.67
Salinas scene Dataset					
Brocoli-green-weeds-1	7	00	00	100	100
Brocoli-green-weeds-2	9.46	9.97	9.97	99.01	100
Fallow	7.80	9.84	9.84	100	100
Fallow-rough-plow	7.13	00.00	00.00	98.90	100
Fallow-smooth	3.80	9.72	9.72	99.65	97.09
Stubble	3.91	00	00	100	100
Celery	5.55	00	00	99.67	100
Grapes-untrained	7.28	9.15	9.15	98.43	100
Soil-vinyard-develop	9.84	00.00	00.00	100.00	100.00
Corn-senesced-green-weeds	3	9.10	9.10	99.45	100
Lettuce-romaine-4wk	9	00	00	100	100
Lettuce-romaine-5wk	9	9.78	9.78	98.99	100
Lettuce-romaine-6wk	0.55	00	00	99.03	97.50
Lettuce-romaine-7wk	3.46	9.21	9.21	99.34	100
Vinyard-untrained	7.47	5.52	5.52	98.67	99.24
Vinyard-vertical-trellis	9.06	9.24	9.24	98.3	100
OA%	9.08	9.10	9.10	99.28	99.71
AA%	3.65	9.47	9.47	99.48	99.61
Kappa%			3.99	99.01	99.67
Pavia University Dataset					
sphalt	4.31	4	9.63	9.45	9.50
leadows	4.32	0	9.87	9.56	9.93
ravel	1.59	1	5.24	9.23	7.96
rees	0.64	00	3.71	3.67	9.46
ainted metal sheets	00	5	9.84	3.45	3.94
are Soil	1.93	7	00.00	00	00
itumen	4.82	5	00.00	00	9.67
elf-Blocking Bricks	0.11	5	9.86	7.85	7.14
hadows	9.55	5	2.78	3.45	4.56
A%	5.11	4	9.07	9.15	9.34
A%	0.81	5	7.99	3.07	3.57
appa%	9.16	1	3.77	9.08	9.13

The proposed segmentation method achieves accurate results than the other methods such as 3D-CNN, 2D-CNN, Hybrid SN, and Spectral CNN [16, 18]. Because, the implemented method ignores the joint features context information without considering the spectral information of the image. The proposed OSegNet based feature extraction method greatly reduces the dimensionality of the database without losing any spatial and spectral information. The accomplished OA, and

AA of the proposed method is 99.13% and 96.58% accordingly.

Fig.6 illustrates the achieved values of different measures for the four systems over test data [16]. From the graph, it is observed that all the four methods implemented equally good. But among the four methods, the proposed OSegNet achieves excellent precision, recall and f1-score values i.e. 98.02%, 99.56% and 99.01% respectively. This proposed method accomplished better classification performance than the other traditional classification models.

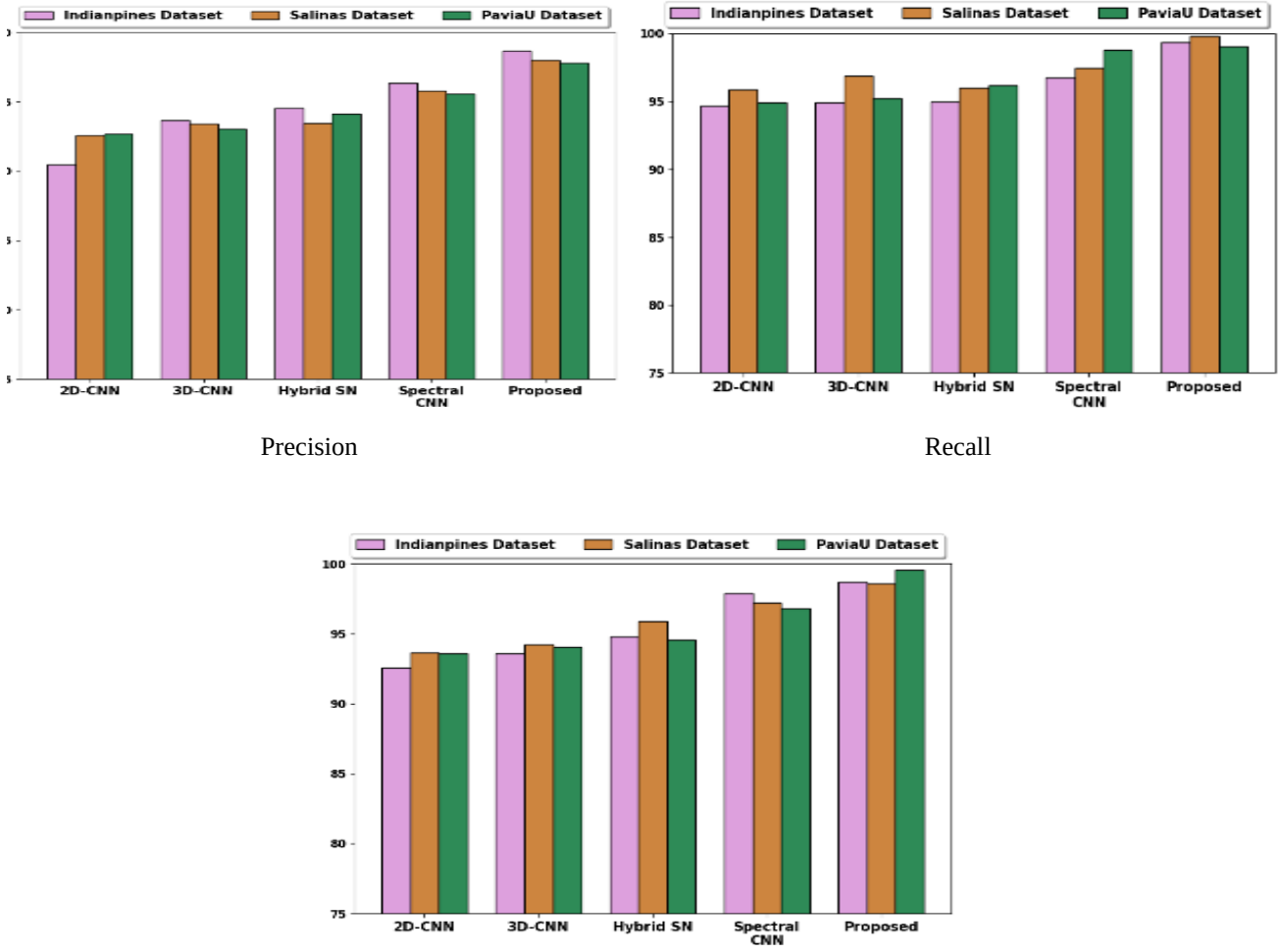

Precision

Recall

F1-score

Fig 6. Performance comparison of proposed method

Table 3 provides the performance measure values of proposed OSegNet and some of the other state-of-art technique values for precision, f1-score, recall, OA, AA, Kappa, training and testing based on IP, PU, and SD datasets [16, 18]. From the table, the training time of the proposed approach over IP, PU, and SD datasets are 250.55 s, 600.78 s, 700.54 s, and 27.89 s correspondingly. Also, Table 3, list out the comparison of proposed method's training and testing time with the existing methods. From the table, it is observed that the running time of the introduced approach is relatively high, but the segmentation and classification outcomes are better.

Fig.7 illustrates the performance measure comparison introduced scheme with some of the previous algorithms [16]. It is clear from the outcomes in Fig.7, that the achieved OA by the five methods maximize with the increasing number of learning rates.

Furthermore, the proposed method has the better performance by varying learning rate step sizes. If the amount of learning rate step size is small, the benefits of OptSegNet is high. However, the achieved values are comparatively maximum than the other methods.

Fig.8 shows the training and testing time complexity comparison of proposed method with various existing methods. The 3D-CNN approach uses minimum training and testing time because, generally the DL schemes consists of more parameters and larger input feature maps [16].

Furthermore, the major objective of the proposed method is to enhance the performance via applying lowest labeled samples and a maximum unlabeled sample, it needs further

training time, but testing time still has one advantage compared with other methods.

Fig.9 demonstrates the performance comparison based on different patch size. In the OptSegNet method, the size of depth-wise convolutional kernel is set experimentally. It is recorded as $D \times D$.

Table 3. Classification Accuracy of IP, SD, and PU Dataset Images of Proposed and Exiting Techniques

Method	Precision%	F1 score%	ecall%	A%	A%	appa%	raining (sec)	esting (sec)
			IP					
3D-CNN [16]	93.67	93.61	4.89	1.10	1.58	9.98	1.18	.23
2D-CNN [16]	90.45	92.56	4.67	9.48	5.14	7.96	3.55	.11
Hybrid SN [16]	94.56	94.78	5	7.57	4.72	7.23	2.85	.92
Spectral CNN	96.34	97.89	5.78	3.06	5.17	7.29		
Proposed	98.67	98.66	9.33	9.13	5.58	9.01	50.55	.30
			SD					
3D-CNN [16]	93.41	94.05	5.23	3.96	7.01	3.32	3.17	.77
2D-CNN [16]	92.58	93.61	4.89	7.38	3.84	7.08	46.91	.95
Hybrid SN [16]	93.45	94.56	5.20	9.10	9.47	3.99	5.37	3.58
Spectral CNN	95.78	96.78	3.78	9.28	9.48	9.01		
Proposed	98.02	99.56	9.01	9.71	9.61	9.67	00.78	.50
			PU					
3D-CNN [16]	93.02	94.23	5.91	5.11	0.81	9.16	3.72	.33
2D-CNN [16]	92.67	93.67	5.89	4	5	1	02.62	.81
Hybrid SN [16]	94.12	95.89	5.02	9.07	7.99	3.77	3.23	3.85
Spectral CNN	95.56	97.19	7.45	9.15	3.07	9.08		
Proposed	97.80	98.56	9.78	9.34	3.57	9.13	00.54	.01

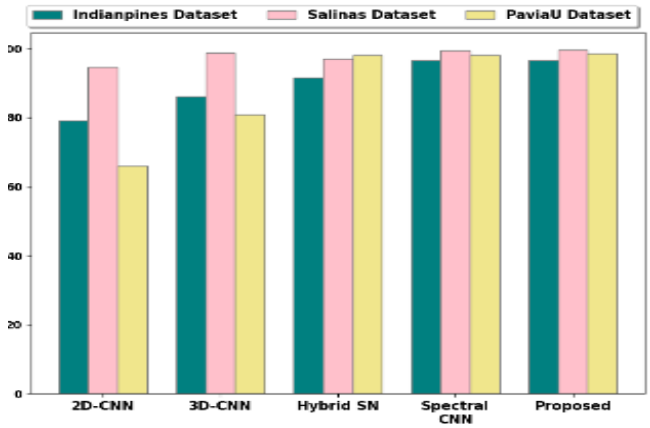

Average Accuracy

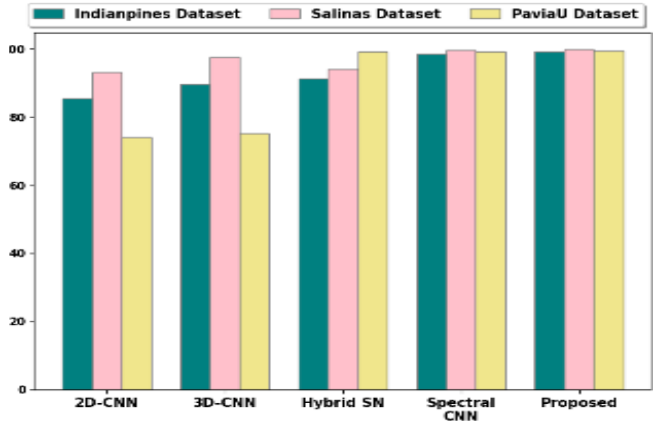

Overall Accuracy

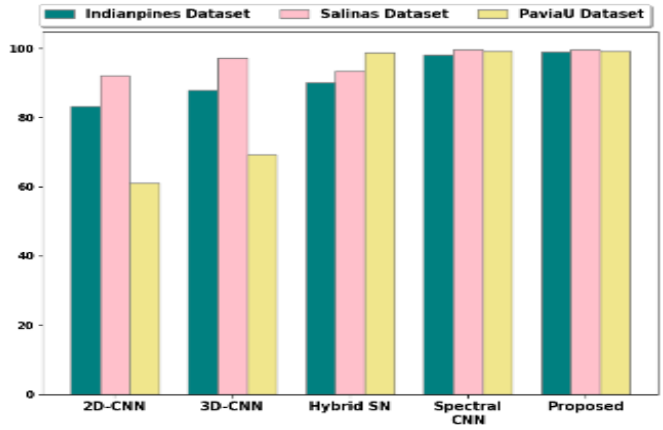

Kappa

Fig 7. Performance analysis of proposed method on IP and Salinas dataset

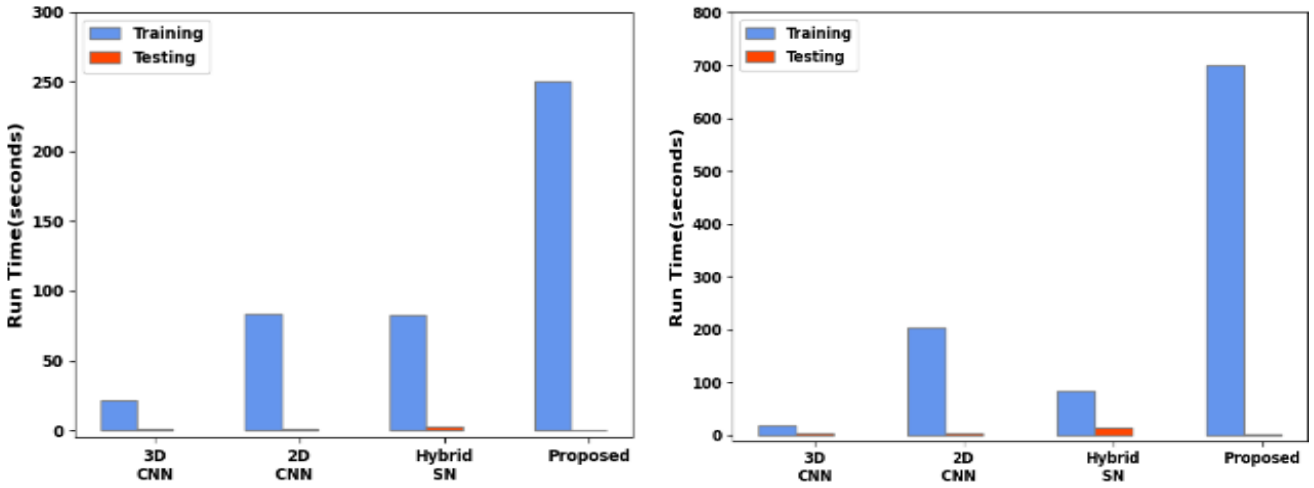

IP PU

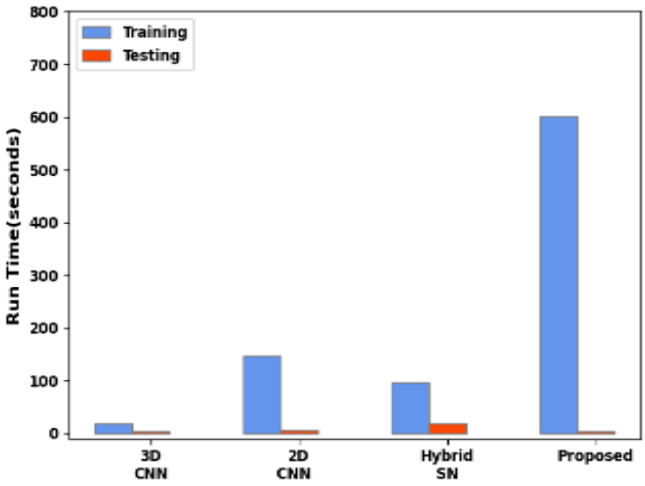

SD

Fig 8. Training and testing time comparison

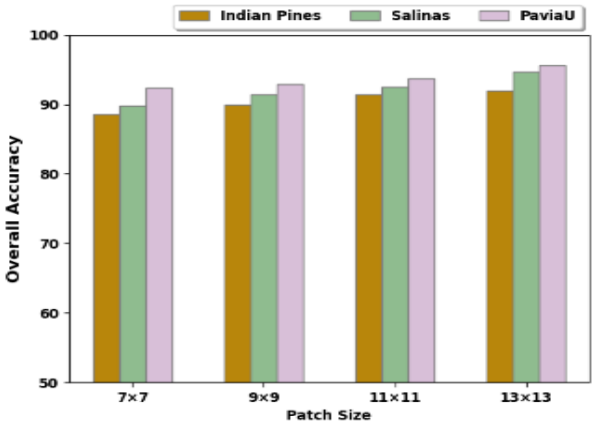

Fig 9. Performance comparison based on varying patch size

4.1.2. Comparison of Segmentation models

It is found that the depth-wise convolutional kernel in the proposed system has the highest impact over the PU database and has lower impact on the other three databases [19]. The parameter D becomes 7, 9, 11 and 13 correspondingly, the segmentation outcomes are shown in Table 4. The maximum OAs are accomplished for all the three databases while the size of the kernel is 13×13. Finally, set the kernel size as 13×13.

Table 4. Achieved Performance Based on Different Patch Size

Patch size	IP%	SD%	PU%
7×7	38.56	39.78	92.43
9×9	39.90	91.45	92.90
11×11	91.45	92.56	93.78
13×13	91.90	94.67	95.67

Fig.10 shows the proposed method performance with and without optimization over other optimization techniques such as IPSO, CS, DE, and FF. From the Table 5, it is observed that the obtained fitness value of the proposed OptSegNet is 3% maximum than the SegNet with MGO for IP dataset. The proposed OptSegNet achieves 19% enhanced fitness outcome than the SegNet-MGO for SD. Finally, the introduced OptSegNet's fitness outcome is 18% maximum than the SegNet-MGO for PU. Therefore, the enhanced optimization algorithm which is applied in the proposed OptSegNet achieves more accurate segmentation results than the other algorithms.

Table 5 represents the achieved fitness value of the proposed OptSegNet i.e. SegNet with EMGO and SegNet-MGO. From the table it is clear that the obtained fitness result of the introduced system is maximum than the other implemented optimization algorithm's fitness values.

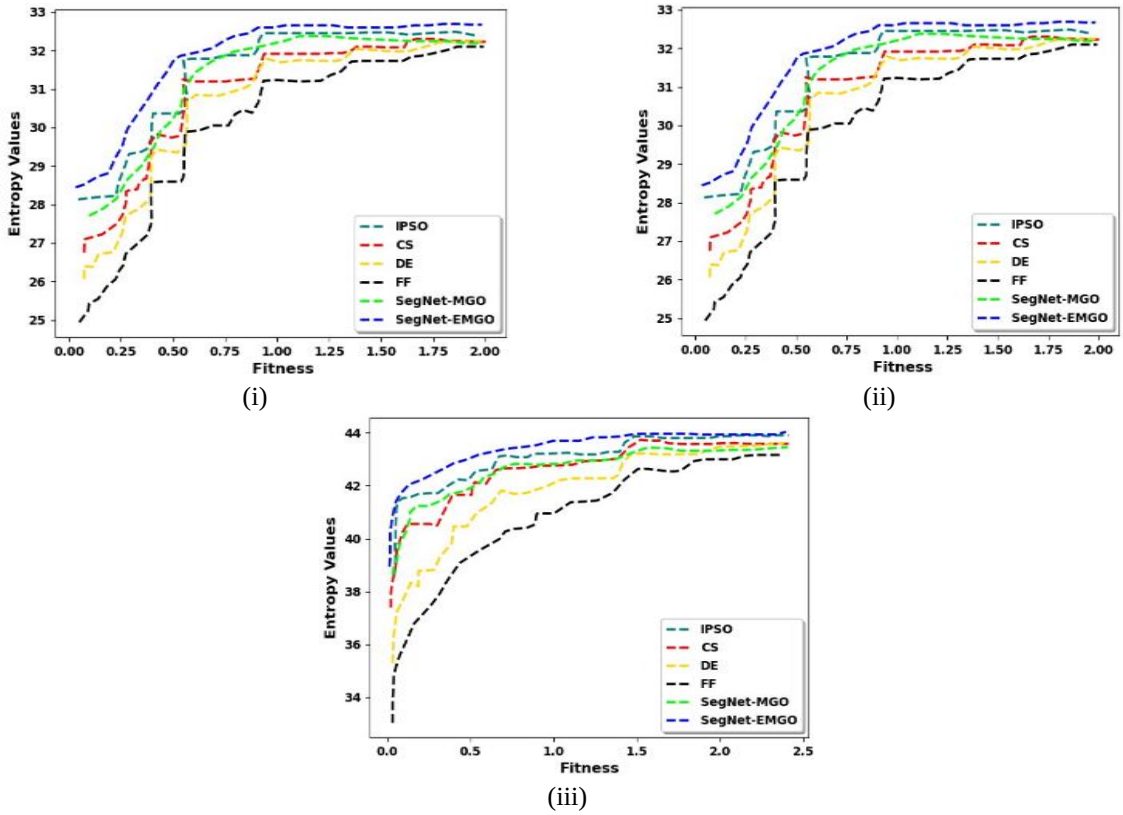

Fig 10. With and without optimization algorithm performance comparison (i) IP, (ii) SD and (iii) PU

Table 5. Optimization Comparison

lethods	egNet-MGO	roposed MGO	SegNet- PSO [21]	S [31]	E [32]	F [33]
)	3.890	5.569	4.619	4.427	3.627	3.554
D	3.129	9.452	3.422	7.689	7.578	5.964
U	1.519	9.120	7.009	5.096	5.446	5.193

Table 6. Segmentation Performance Comparison for IP, PU and SD Based 5% And 15% Training Samples.

lgorithms	A (5%)	A (5%)	appa (5%)	A (15%)	A (15%)	appa (15%)
)						
lexNet [34]	689	5692	6450	8167	7955	7907
esNet [35]	707	6996	6640	8300	8067	8059
enseNet [36]	711	6732	6683	8428	8149	8203
RAN [37]	727	7359	6975	8286	7663	8039
SSFNet [38]	737	6795	6998	8261	7448	8005
roposed	907	9367	92867	9234	956	956
D						
lexNet [34]	9290	9182	9056	9298	9359	9149
esNet [35]	9090	9142	8785	9424	9489	9322
enseNet [36]	9036	8951	8719	9239	9355	9145
RAN [37]	9359	9247	9151	9482	9362	9314
SSFNet [38]	9372	9235	9165	9437	9265	9252
roposed	947	987	9878	961	9534	9825
U						
lexNet [34]	9419	9676	9353	9437	9579	9531
esNet [35]	9180	9529	9087	9379	9685	9309
enseNet [36]	9114	9447	9012	9309	9605	9229
RAN [37]	9033	8823	8922	9195	8944	9102
SSFNet [38]	9356	9669	9282	9585	9803	9537
roposed	9483	9750	9550	9612	9831	9611

Table 6 illustrates that the performance of the proposed OSegNet is higher than the other conventional segmentation models through 5% and 15% based on OA, AA and Kappa. This introduced segmentation system demonstrates the excellent results over three different datasets.

Fig.11 (a), (d), and (g) illustrates the achieved AA, Kappa, and OA measures of proposed for IP, (b), (e), and (h) illustrates the achieved AA, Kappa, and OA measures of proposed for PU.

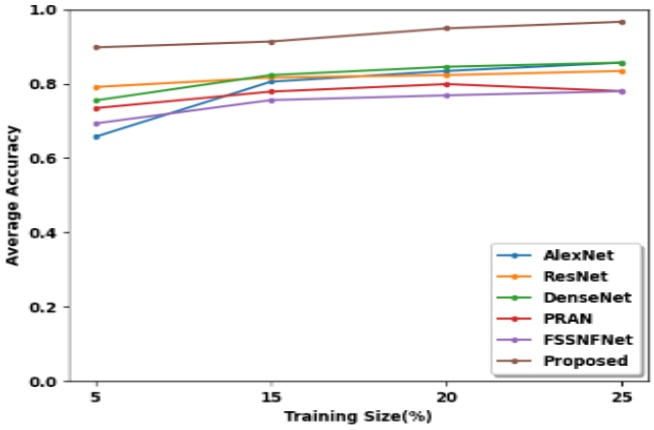
Average Accuracy
Training Size(%)
AlexNet
ResNet
DenseNet
PRAN
FSSNFNet
Proposed

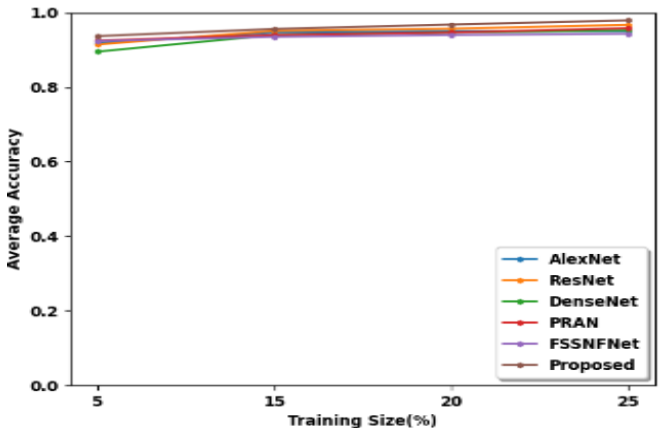
Average Accuracy
Training Size(%)
AlexNet
ResNet
DenseNet
PRAN
FSSNFNet
Proposed

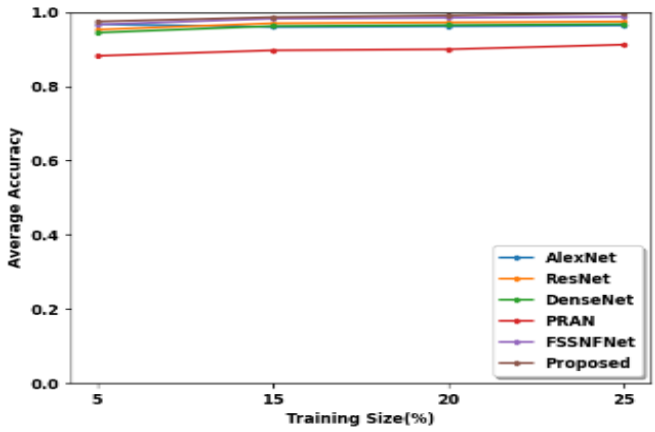
Average Accuracy
Training Size(%)
AlexNet
ResNet
DenseNet
PRAN
FSSNFNet
Proposed

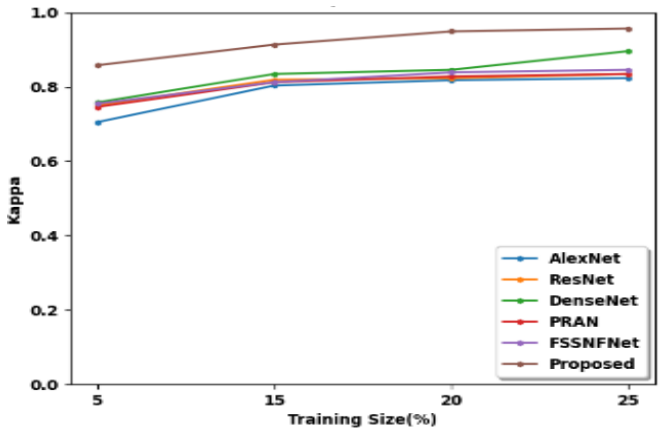
Kappa
Training Size(%)
AlexNet
ResNet
DenseNet
PRAN
FSSNFNet
Proposed

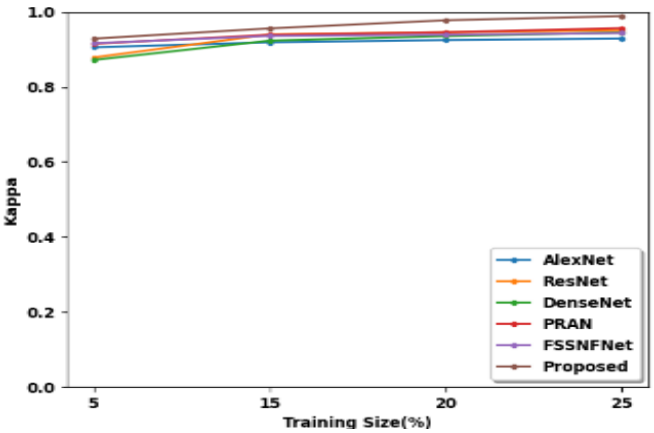
Kappa
Training Size(%)
AlexNet
ResNet
DenseNet
PRAN
FSSNFNet
Proposed

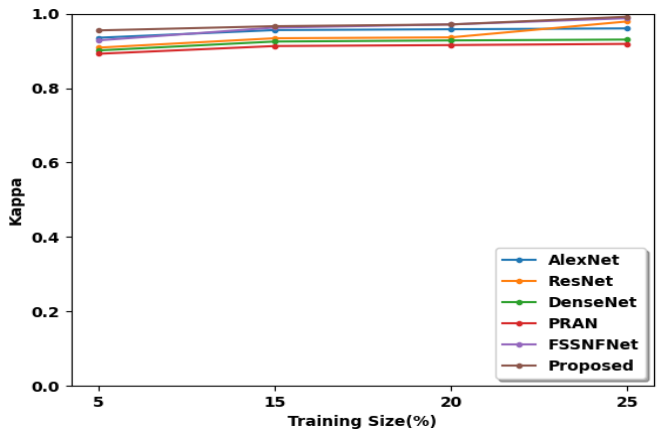
Kappa
Training Size(%)
AlexNet
ResNet
DenseNet
PRAN
FSSNFNet
Proposed

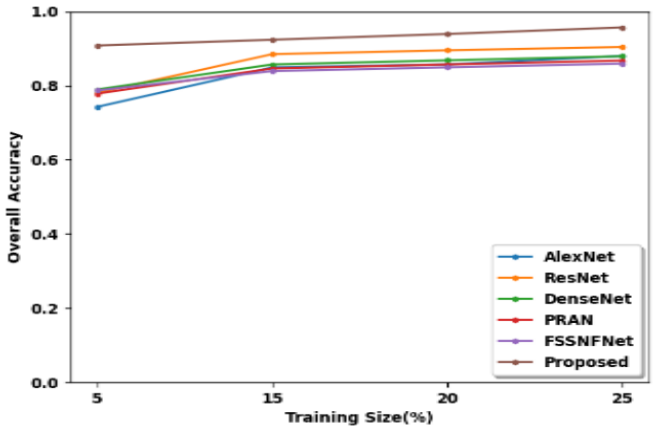
Overall Accuracy
Training Size(%)
AlexNet
ResNet
DenseNet
PRAN
FSSNFNet
Proposed

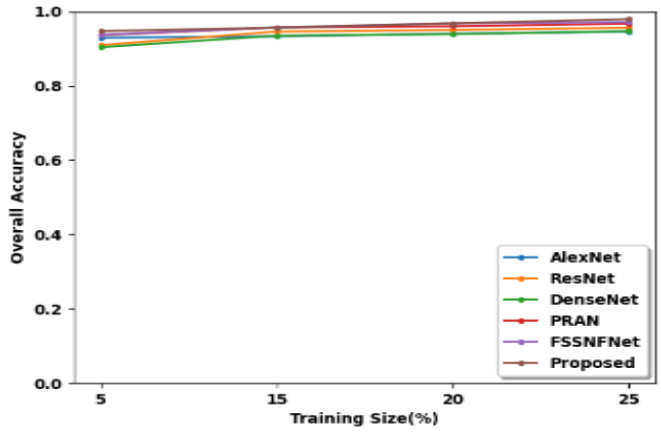
Overall Accuracy
Training Size(%)
AlexNet
ResNet
DenseNet
PRAN
FSSNFNet
Proposed

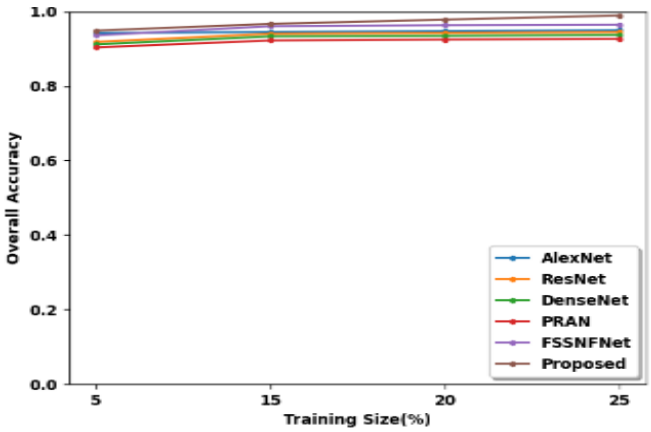

Fig 11. Comparison of segmentation models

Further, Fig.11 (c), (f), and (i) illustrates the achieved AA, Kappa, and OA measures of proposed for SD compared with some traditional segmentation methods such as AlexNet [34], ResNet [35], DenseNet [36], PRAN [37], and FSSNFNet [38]. Proposed method attains best segmentation results when the training sample is 5% and 15%.

5. Conclusion

This research work incorporates dual UNet with the ResNet_50 for RSI segmentation and proposes a feature extraction and segmentation-based OptSegNet model. Especially in the dual UNet with ResNet_50 network, depth-wise convolution is designed to extract the joint features of RSIs. Finally, the output of decoder module 2 (UNet2) is concatenated with the output of decoder module 1 (UNet1) which produces an accurate segmentation outcome than the other implemented models. The experimental outcome shows that the OptSegNet performs well with satisfactory performance for the three databases. The proposed technique is implemented in PYTHON platform. Finally, the achieved OA, AA, and kappa values of proposed method on IP dataset is 99.13%, 96.58% and 100%. On SD is 99.71%, 99.61% and 99.67%, on PU is 99.34%, 98.57%, and 99.13% respectively. In the future work, as different unlabeled samples are applied to enhance the learning performance, it will explore how to minimize training time.

Reference

[1] S. Illarionova, D. Shadrin, A. Trekin, V. Ignatiev, and I. Oseledets, "Generation of the NIR spectral band for satellite images with Convolutional Neural Networks," Sensors, vol. 21, no. 16, p. 5646, 2021. doi:10.3390/s21165646

[2] K. Yuan et al., "Deep-learning-based multispectral satellite image segmentation for water body detection," IEEE Journal of Selected Topics in Applied Earth Observations and Remote Sensing, vol. 14, pp. 7422–7434, 2021. doi:10.1109/jstars.2021.3098678

[3] Y. Chen, Q. Weng, L. Tang, Q. Liu, and R. Fan, "An automatic cloud detection neural network for high-resolution remote sensing imagery with cloud–snow coexistence," IEEE Geoscience and Remote Sensing Letters, vol. 19, pp. 1–5, 2022. doi:10.1109/lgrs.2021.3102970

[4] L. Yin et al., "Haze grading using the Convolutional Neural Networks," Atmosphere, vol. 13, no. 4, p. 522, 2022. doi:10.3390/atmos13040522

[5] X. Xu et al., "A novel approach for scene classification from remote sensing images using Deep Learning Methods," European Journal of Remote Sensing, vol. 54, no. sup2, pp. 383–395, 2020. doi:10.1080/22797254.2020.1790995

[6] D. Rashkovetsky, F. Mauracher, M. Langer, and M. Schmitt, "Wildfire detection from multisensor satellite imagery using deep semantic segmentation," IEEE Journal of Selected Topics in Applied Earth Observations and Remote Sensing, vol. 14, pp. 7001–7016, 2021. doi:10.1109/jstars.2021.3093625

[7] Q. Hu, L. Zhen, Y. Mao, X. Zhou, and G. Zhou, "Automated building extraction using satellite remote sensing imagery," Automation in Construction, vol. 123, p. 103509, 2021. doi:10.1016/j.autcon.2020.103509

[8] A. Sharifi, H. Mahdipour, E. Moradi, and A. Tariq, "Agricultural Field extraction with deep learning algorithm and satellite imagery," Journal of the Indian Society of Remote Sensing, vol. 50, no. 2, pp. 417–423, 2022. doi:10.1007/s12524-021-01475-7

[9] L. Yao, T. Liu, J. Qin, N. Lu, and C. Zhou, "Tree counting with high spatial-resolution satellite imagery based on Deep Neural Networks," Ecological Indicators, vol. 125, p. 107591, 2021. doi:10.1016/j.ecolind.2021.107591

[10] S. Baroud, S. Chokri, S. Belhaous, and M. Mestari, "A brief review of graph convolutional neural network

based learning for classifying remote sensing images," Procedia Computer Science, vol. 191, pp. 349–354, 2021. doi:10.1016/j.procs.2021.07.047

[11] X. Yu et al., "NestNet: A multiscale convolutional neural network for Remote Sensing Image Change Detection," International Journal of Remote Sensing, vol. 42, no. 13, pp. 4898–4921, 2021. doi:10.1080/01431161.2021.1906982

[12] S. Gadamsetty, R. Ch, A. Ch, C. Iwendi, and T. R. Gadekallu, "Hash-based deep learning approach for remote sensing satellite imagery detection," Water, vol. 14, no. 5, p. 707, 2022. doi:10.3390/w14050707

[13] K. A. Korznikov et al., "Using u-net-like deep convolutional neural networks for precise tree recognition in very high resolution RGB (red, green, blue) satellite images," Forests, vol. 12, no. 1, p. 66, 2021. doi:10.3390/f12010066

[14] A. Abdollahi, B. Pradhan, and N. Shukla, "Road extraction from high-resolution orthophoto images using convolutional neural network," Journal of the Indian Society of Remote Sensing, vol. 49, no. 3, pp. 569–583, 2020. doi:10.1007/s12524-020-01228-y

[15] X. Wu, D. Hong, and J. Chanussot, "Convolutional Neural Networks for Multimodal Remote Sensing Data Classification," IEEE Transactions on Geoscience and Remote Sensing, vol. 60, pp. 1–10, 2022. doi:10.1109/tgrs.2021.3124913

[16] L. Zhou et al., "Shallow-to-deep spatial–spectral feature enhancement for Hyperspectral Image Classification," Remote Sensing, vol. 15, no. 1, p. 261, 2023. doi:10.3390/rs15010261

[17] C. Zhao, B. Qin, S. Feng, and W. Zhu, "Multiple Superpixel graphs learning based on adaptive multiscale segmentation for Hyperspectral Image Classification," Remote Sensing, vol. 14, no. 3, p. 681, 2022. doi:10.3390/rs14030681

[18] E. Ravi Kondal and S. Sankar Barpanda, "Hyperspectral image classification using HYB-3D convolution neural network spectral partitioning," Indonesian Journal of Electrical Engineering and Computer Science, vol. 29, no. 1, p. 295, 2022. doi:10.11591/ijeecs.v29.i1.pp295-303

[19] L. Song, Z. Feng, S. Yang, X. Zhang, and L. Jiao, "Self-supervised assisted semi-supervised Residual Network for Hyperspectral Image Classification," Remote Sensing, vol. 14, no. 13, p. 2997, 2022. doi:10.3390/rs14132997

[20] A. Zhang et al., "Superpixel nonlocal weighting joint sparse representation for hyperspectral image classification," Remote Sensing, vol. 14, no. 9, p. 2125, 2022. doi:10.3390/rs14092125

[21] R. Chakraborty, R. Sushil, and M. L. Garg, "Hyperspectral image segmentation using an improved PSO aided with multilevel fuzzy entropy," Multimedia Tools and Applications, vol. 78, no. 23, pp. 34027–34063, 2019. doi:10.1007/s11042-019-08114-x

[22] Z. Wang, C. Zou, and W. Cai, "Small sample classification of hyperspectral remote sensing images based on Sequential Joint Deeping Learning model," IEEE Access, vol. 8, pp. 71353–71363, 2020. doi:10.1109/access.2020.2986267

[23] Z. He, H. Wu, and G. Wu, "Spectral-spatial classification of hyperspectral images using label dependence," IEEE Access, vol. 9, pp. 119219–119231, 2021. doi:10.1109/access.2021.3107976

[24] T. Zhao and S.-X. Zhang, "X-ray image enhancement based on nonsubsampled shearlet transform and gradient domain guided filtering," Sensors, vol. 22, no. 11, p. 4074, 2022. doi:10.3390/s22114074

[25] S. Q. Nisa and A. R. Ismail, "Dual U-Net with resnet encoder for segmentation of medical images," International Journal of Advanced Computer Science and Applications, vol. 13, no. 12, 2022. doi:10.14569/ijacsa.2022.0131265

[26] B. Abdollahzadeh, F. S. Gharehchopogh, N. Khodadadi, and S. Mirjalili, "Mountain Gazelle optimizer: A new nature-inspired metaheuristic algorithm for global optimization problems," Advances in Engineering Software, vol. 174, p. 103282, 2022. doi:10.1016/j.advengsoft.2022.103282

[27] Q. Li, Y. Shi, X. Huang, and X. X. Zhu, "Building footprint generation by integrating convolution neural network with feature Pairwise Conditional Random Field (FPCRF)," IEEE Transactions on Geoscience and Remote Sensing, vol. 58, no. 11, pp. 7502–7519, 2020. doi:10.1109/tgrs.2020.2973720

[28] https://paperswithcode.com/dataset/indian-pines

[29] https://paperswithcode.com/dataset/salinas

[30] https://paperswithcode.com/dataset/pavia-university

[31] S. Agrawal, R. Panda, S. Bhuyan, and B. K. Panigrahi, "Tsallis entropy based optimal multilevel Thresholding using cuckoo search algorithm," Swarm and Evolutionary Computation, vol. 11, pp. 16–30, 2013. doi:10.1016/j.swevo.2013.02.001

[32] S. Sarkar, S. Paul, R. Burman, S. Das, and S. S. Chaudhuri, "A fuzzy entropy based multi-level image thresholding using differential evolution," Swarm,

Evolutionary, and Memetic Computing, pp. 386–395, 2015. doi:10.1007/978-3-319-20294-5_34

[33] S. Pare, A. K. Bhandari, A. Kumar, and G. K. Singh, "A new technique for multilevel color image thresholding based on modified fuzzy entropy and Lévy flight Firefly algorithm," Computers & Electrical Engineering, vol. 70, pp. 476–495, 2018. doi:10.1016/j.compeleceng.2017.08.008

[34] M. Salman and S. E. Yuksel, "Fusion of hyperspectral image and Lidar data and classification using deep convolutional Neural Networks," 2018 26th Signal Processing and Communications Applications Conference (SIU), 2018. doi:10.1109/siu.2018.8404199

[35] M. E. Paoletti et al., "Deep pyramidal residual networks for spectral–spatial hyperspectral image classification," IEEE Transactions on Geoscience and Remote Sensing, vol. 57, no. 2, pp. 740–754, 2019. doi:10.1109/tgrs.2018.2860125

[36] G. Yang, U. B. Gewali, E. Ientilucci, M. Gartley, and S. T. Monteiro, "Dual-channel densenet for hyperspectral image classification," IGARSS 2018 - 2018 IEEE International Geoscience and Remote Sensing Symposium, 2018. doi:10.1109/igarss.2018.8517520

[37] H. Gao, Y. Yang, D. Yao, and C. Li, "Hyperspectral image classification with pre-activation residual attention network," IEEE Access, vol. 7, pp. 176587–176599, 2019. doi:10.1109/access.2019.2957163

[38] J. Chen, S. Chen, P. Zhou, and Y. Qian, "Deep Neural Network based hyperspectral pixel classification with factorized spectral-spatial feature representation," IEEE Access, vol. 7, pp. 81407–81418, 2019. doi:10.1109/access.2019.2923776

[39] D. Datta, P. K. Mallick, D. Gupta, and G.-S. Chae, "Hyperspectral image classification based on novel hybridization of spatial-spectral-superpixelwise principal component analysis and dense 2D-3D convolutional neural network fusion architecture," Canadian Journal of Remote Sensing, vol. 48, no. 5, pp. 663–680, 2022. doi:10.1080/07038992.2022.2114440

[40] C. Mu, Z. Dong, and Y. Liu, "A two-branch convolutional neural network based on multi-spectral entropy rate Superpixel segmentation for hyperspectral image classification," Remote Sensing, vol. 14, no. 7, p. 1569, 2022. doi:10.3390/rs14071569

[41] S.S. Alegavi, R.R. Sedamkar, "Implementation of Deep Convolutional Neural Network for Classification of Multiscaled & Multiangled Remote Sensing Scene", International Journal on Soft Computing approaches for image analysis in practical scenario: Challenges, Solutions and Applications, Intelligent Decision Technologies, 14 (2020) 21–34, DOI: 10.3233/IDT-190076 IOS Press February 2020.

[42] S. S. Alegavi and R.R. Sedamkar, "Research Trends in Hyperspectral Imagery Data" International Journal of Computer Engineering & Technology (IJCET), (UGC Approved Journal), ISSN Print: 0976 – 6367, ISSN Online: 0976 – 6375, IJCET, Volume 10, Issue 2, Article Id., IJCET_10_02_008, IAEME Publications, pg. no. 67-73, March-April 2019.

[43] Sherje, N. P., Agrawal, S. A., Umbarkar, A. M., Kharche, P. P., & Dhabliya, D. (2021). Machinability study and optimization of CNC drilling process parameters for HSLA steel with coated and uncoated drill bit. Materials Today: Proceedings, doi:10.1016/j.matpr.2020.12.1070

[44] Paul Garcia, Anthony Walker, Luis Gonzalez, Carlos Pérez, Luis Pérez. Improving Question Generation and Answering Systems with Machine Learning. Kuwait Journal of Machine Learning, 2(2). Retrieved from http://kuwaitjournals.com/index.php/kjml/article/view/187

[45] Matti Virtanen, Jan de Vries, Thomas Müller, Daniel Müller, Giovanni Rossi. Machine Learning for Intelligent Feedback Generation in Online Courses . Kuwait Journal of Machine Learning, 2(2). Retrieved from http://kuwaitjournals.com/index.php/kjml/article/view/188